Synthesis and application of a novel nanomagnetic catalyst with Cl[DABCO-NO_2]$C(NO_2)_3$ tags in the preparation of pyrazolo[3,4-*b*]-pyridines via anomeric based oxidation

Javad Afsar,[a] Mohammad Ali Zolfigol,*[a] Ardeshir Khazaei,*[a] Diego A. Alonso, *[b] Abbas Khoshnood *[b], Yadollah Bayat, [c] Asiye Asgari[c]

[a]*Department of Organic Chemistry, Faculty of Chemistry, Bu-Ali Sina University, Hamedan, 6517838683, Iran.*

[b]*Organic Chemistry Department and Organic Synthesis Institute, Alicante University, Apdo. 99, 03080 Alicante, Spain.*

[c]*Faculty of Chemistry and chemical Engineering, Malek Ashtar University of Technology, Tehran, Iran.*

**Corresponding author(s): E-mail:* zolfi@basu.ac.ir, mzolfigol@yahoo.com*;* Khazaei_1326@yahoo.com*;diego.alonso@ua.es (Diego A. Alonso) and abbas.khoshnood@ua.es (Abbas Khoshnood), Fax: +98 8138380709; Tel: +98 8138282807.*

Abstract: A novel nanomagnetic catalyst with Cl[DABCO-NO_2]$C(NO_2)_3$ tags was designed, synthesized and fully characterized by several identical techniques such as Fourier transform spectroscopy infrared (FT-IR), Energy-dispersive X-ray spectroscopy (EDX), elemental mapping analysis, thermal gravimetry analysis (TG), derivative thermal gravimetric (DTG), powder X-ray diffraction patterns (XRD), Field scanning electron microscopy (FESEM), high resolution transmission electron microscopy (HRTEM), physical adsorption and physisorption of N_2 isotherms (BET) and vibrating sample magnetometer (VSM). The mentioned nano-magnetic

particles were used as an efficient and recyclable catalyst for the one-pot three component condensation reaction of 5-amino-3- methyl-1-phenylpyrazole, aryl aldehydes and malononitrile for the synthesis of pyrazolo[3,4-*b*]-pyridine derivatives under neat condition.

Introduction

Nowadays, chemical processes that produce the least waste and pollutants are paramount important. One of the ways to achieve this great goal is to use catalysts. Catalysts increase chemical reactions rate by reducing the corresponding activation energy, which reduces energy consumption [1]. Homogeneous catalysts have a good performance in chemical processes, but their separation from the reaction mixture is tediously long, so the use of heterogeneous catalysts is replaced [2]. In order to increase the efficiency of heterogeneous catalysts, they can be designed in nano dimensions [3, 4]. But nano-sized catalysts cannot be separated by conventional filtration techniques. Then, nano-magnetic catalysts are designed to solve the mentioned problem. Generally, these catalysts can be easily separated by using an usual external magnetic field from the reaction and reused several times with only a marginal decrease in reactivity [5,6].

In order to increase the efficiency of chemical reactions, simplify the process, saving time and energy, increasing the atomic economy, reducing use of organic solvents and waste generation, multi-component reactions (MCRs) are introduced. Therefore, the intention of MCRs is important in the synthetic organic methodologies [7,8].

The anomeric effect is one of the most important fundamental factors which are influencing the reactivity of susceptible systems. This concept has been extensively reviewed to discuss the origin, magnitude, scope and limitations of this important phenomenon in various systems [9-12].

Anomeric effect is considered for justifying some observations in chemistry. This phenomenon, which is caused by the interaction between the lone pair electrons of the heteroatoms and the

antibonding orbital of the adjacent bonds, can affect the pathway of the reaction mechanism, causing the abnormal hydride transfer following releasing of a hydrogen gas. Recently, a new terminology entitled "anomeric based oxidation (ABO)" has been introduced for driving force of aromatization in susceptible heterocyclic compounds which have heteroatoms at the appropriate sites. Other than experimental observations, computational evidence also confirms this mechanism [13].

The systematic study of the anomeric effect in target molecules, allows for the design of synthetic strategies based on anomerically driven stereoselective reactions, or highly biased equilibria among isomeric products. To the best of our knowledge, many biological processes involve oxidation-reduction of substrates by NAD^+/NADH and/or $NADP^+$/NADPH respectively (**Figure 1**). The key feature of the oxidation mechanism in these systems is hydride transfering from carbon to substrates via anomeric based oxidation. Thus, development of anomeric based oxidation and/or aromatization mechanism lead to knowledge based designing of biomimetic reactions in the future. We think that the obtained results from this field of research will be support the idea of rational designs, syntheses and applications of tasked-specific catalysts and molecules for the development of anomeric based oxidation and/or aromatization mechanism [14-17].

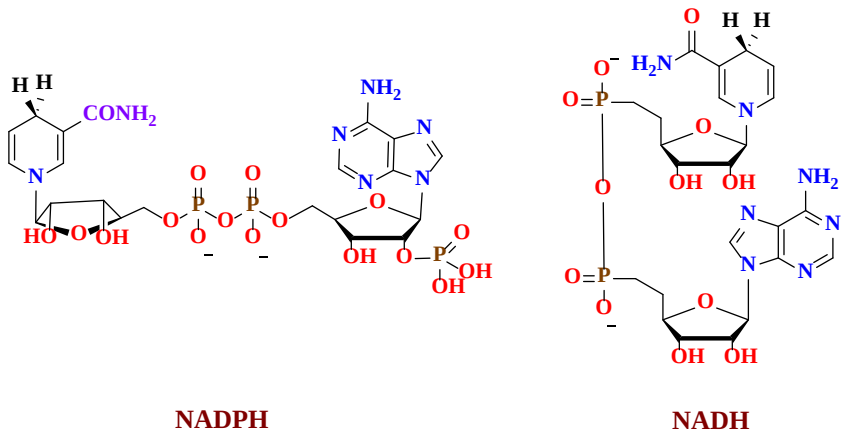

Figure 1. Molecular structures of NADH and NADPH

Pyrazole derivatives have attracted great interest due to the variety of biological and pharmacological activities such as antiviral [18], antidiabetic, [19], hypotensive [20], anticancer [21] antitumor, antibacterial [22] and anti-inflammatory [23]. These compounds also can be effective in the remedy of gastrointestinal disease, drug and alcohol withdrawal symptoms, anorexia nervosa depression, hemorrhaged stress, Alzheimer's disease, infertility and drug addiction [24, 25]. It has recently been found that pyrazolo[3,4-*b*]-pyridines can be also used as FGFR Kinase Inhibitors [26] and metabotropic glutamate receptor 5 (mGluR5) [27] (**Figure 2**). Therefore, due to these important biological abilities, any development in the synthetic organic methodology for preparation of these compounds is great demanded.

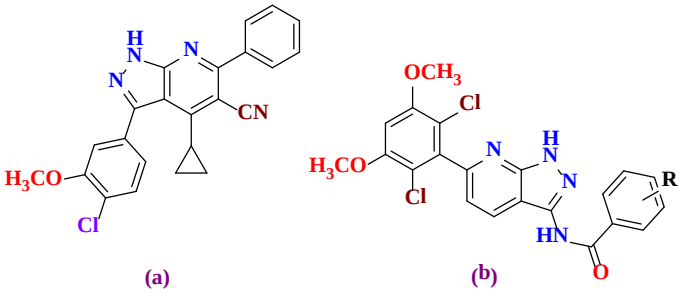

Figure 2. (a) FGFR Kinase Inhibitors (b) metabotropic glutamate receptor 5 (mGluR5)

With this aim, we wish to introduce Fe_2O_3@$SiO_2(CH_2)_3$-Cl[DABCO-NO_2]C$(NO_2)_3$ as a novel nanomagnetic catalyst and use it as an efficient and reusable catalyst in the synthesis of pyrazolo[3,4-*b*]-pyridine derivatives via anomeric based oxidation under solvent-free condition (**Scheme 1**).

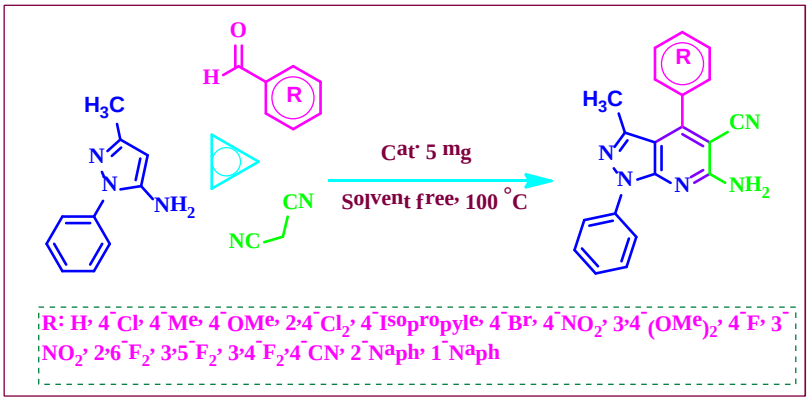

Scheme 1. MCRs Synthesis of pyrazolo[3,4-*b*]-pyridine derivatives using Fe_2O_3@$SiO_2(CH_2)_3$-Cl[DABCO-NO_2]C$(NO_2)_3$ as novel nano magnetic catalyst under solvent free conditions.

The outlook of chemical processes is moving towards the goal of sustainable development. With this aim, the design, synthesis and applications of “benign” catalysts have been one of the serious challenges for chemists and chemical engineers since many years ago. Due to the important role of catalysts in chemical processes, design, synthesis and application of new catalysts are great attracted. Among of catalysts, nano magnetic catalysts have attracted much attention due to their efficient properties such as reusability, easy separation and eco-friendly nature. So, Fe_2O_3@$SiO_2(CH_2)_3$-Cl[DABCO-NO_2]C$(NO_2)_3$ was designed, synthesized and fully characterized by identification techniques. This novel nano magnetic catalyst was used in the synthesis of pyridine derivatives as biological and pharmaceutical candidate drugs.

Results and discussion

Synthesis and Characterization of the novel nano magnetic catalyst

Our strategy for the synthesis of magnetic nanoparticles functionalized DABCO double ionic liquids tags (Fe_2O_3@$SiO_2(CH_2)_3$-Cl[DABCO-NO_2]$C(NO_2)_3$) has been shown in **Scheme 2**.

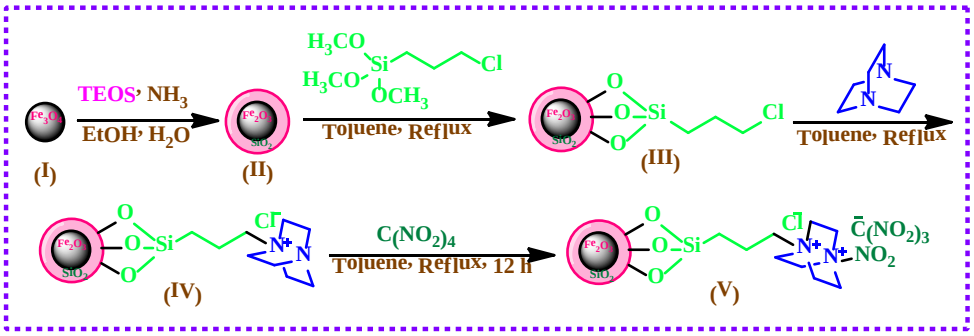

Scheme 2. Synthetic route for Synthesis of novel nano magnetic catalyst Fe_2O_3@$SiO_2(CH_2)_3$-Cl[DABCO-NO_2]$C(NO_2)_3$.

As shown in **Scheme 2**, the DABCO double ionic liquids tags functionalization of magnetic nanoparticles (MNPs) can be achieved in a four step process. First of all, synthesis of core/shell Fe_2O_3@SiO_2 was done by known method based on the literature with some modification (**II**). Moreover, functionalization of magnetic nano particles with silylpropylchloride linker was done by using 3-chloropropyltrimethoxysilane (**III**). Then, DABCO as a double head tertiary amine ligand was entered to the magnetic nanoparticles by reflux in toluene (**III**) and through this way, the first ionic liquids tags was presented. Finally, DABCO-functionalized magnetic nanoparticles (**IV**) were reacted with $C(NO_2)_4$ to transfer one of the acidic NO_2 groups and coordinated to the second amine of DABCO (**V**).

For confirmation the successful synthesis of the catalyst, the structure of the novel nano magnetic heterogeneous catalyst was fully characterized by various techniques such as Fourier transform spectroscopy infrared (FT-IR), elementals mapping survey with energy-dispersive X-ray spectroscopy (EDX), thermal gravimetry analysis (TGA), derivative thermal gravimetric (DTG), powder X-ray diffraction patterns (XRD), Field scanning electron microscopy (FESEM), high resolution transmission electron microscopy (HRTEM), Physical adsorption and physisorption of N_2 isotherms (BET) and vibrating sample magnetometer (VSM).

The FT-IR spectrum of the novel nano magnetic catalyst and its comparison with starting materials is presented in Figure 3. As shown in Figure 3, the peak observed at 586 cm^{-1} is related to the formation of magnetic nanoparticles which is attributed to the Fe-O bonds. The depicted sharp and broad band at 1076 is related to Si-O-Si stretching in silica layer. the absorption bond at 1384 cm^{-1} and 1629 cm^{-1} is connected to the vibrational modes of the -NO_2 bonds. Also, the peak that recognized at 1715 cm^{-1} has been disappeared in Fe_2O_3@$SiO_2(CH_2)_3$-Cl[DABCO] catalyst (**Figure 3**).

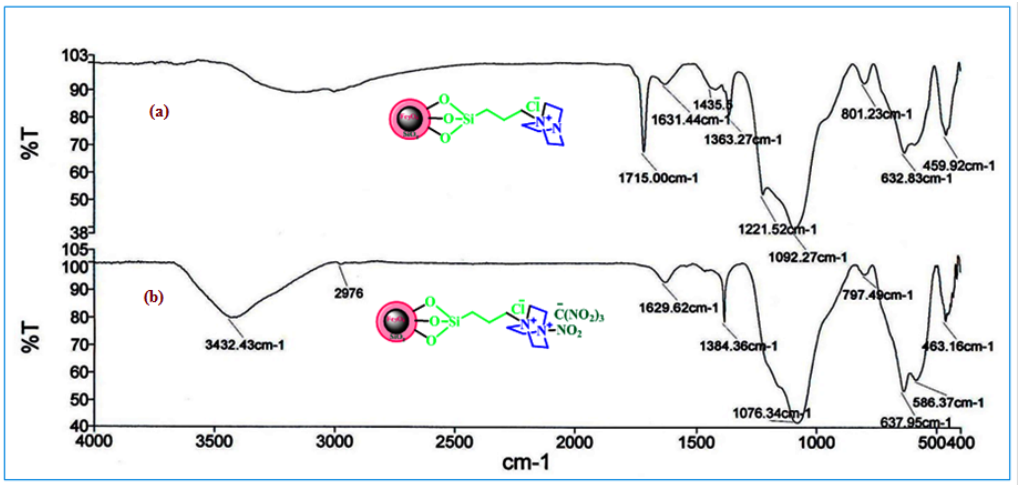

Figure 3. The FT-IR spectrum of a) Fe_2O_3@$SiO_2(CH_2)_3$-Cl[DABCO], and b) Fe_2O_3@$SiO_2(CH_2)_3$-Cl[DABCO-NO_2]$C(NO_2)_3$.

Next, the Energy-dispersive X-ray spectroscopy (EDX) and elemental mapping analysis were used to prove the organic content and also the existence of elemental composition of the MNPs, which could be explained by the DABO ionic liquid tags attache to the MNPs (**Figures 4a-h**). As shown, the results confirmed the presence of carbon (C: 23.73%), nitrogen (N: 12.70%), oxygen (O: 48.33%), Chloride (Cl: 0.06%), Iron (Fe: 11.63%) and Silisum (Si: 3.56%), as the expected elements in the catalyst structure. morover, the selected- area elemental analysis displays the regular uniformity of the synthesized MNPs.

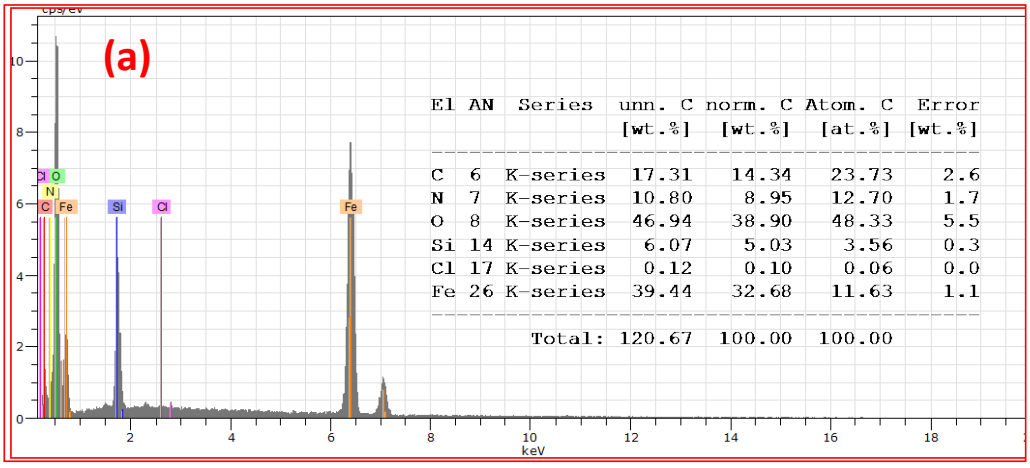

El	AN	Series	unn. C [wt.%]	norm. C [wt.%]	Atom. C [at.%]	Error [wt.%]
C	6	K-series	17.31	14.34	23.73	2.6
N	7	K-series	10.80	8.95	12.70	1.7
O	8	K-series	46.94	38.90	48.33	5.5
Si	14	K-series	6.07	5.03	3.56	0.3
Cl	17	K-series	0.12	0.10	0.06	0.0
Fe	26	K-series	39.44	32.68	11.63	1.1
		Total:	120.67	100.00	100.00	

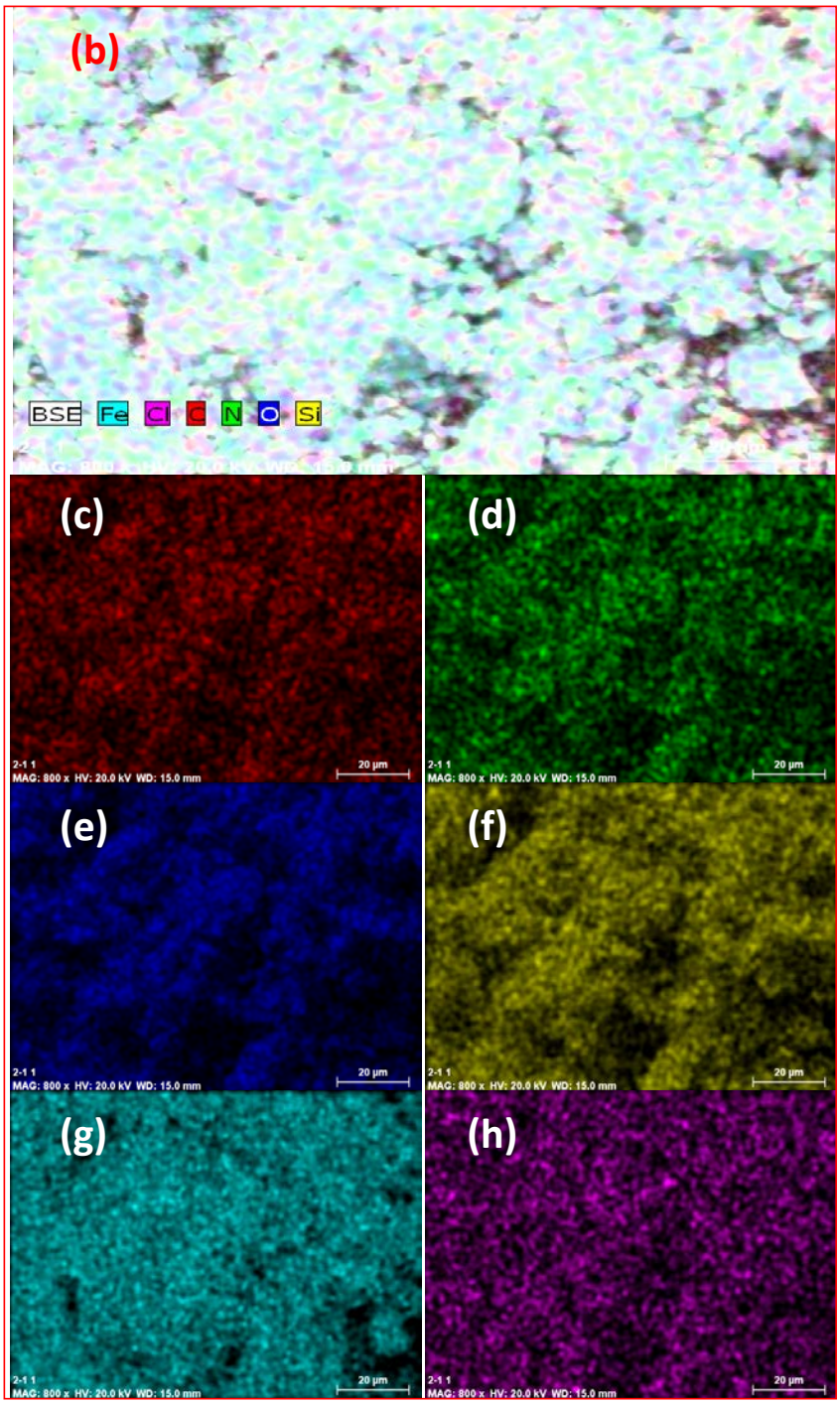
(b)
BSE Fe Cl C N O Si
(c)
(d)
(e)
(f)
(g)
(h)
2-1 1
MAG: 800 x HV: 20.0 kV WD: 15.0 mm
20 µm

Figure 4. a)The EDX spectroscopy quantitative; b) total elemental maps and displays of C (c), N (d), O (e), Si (f), Fe (g), and Cl (h) atoms in the MNPs of catalyst.

To investigate the morphology, topography and resolve the interior of the structures in the final catalyst, high-resolution transmission electron microscopy (HRTEM) and Field emission scanning electron microscopy (FESEM) were carried out as shown in (**Figure 5**). As it is clear in the figure a,b, with presents of SiO_2 layers to disorganized and uneven Fe_2O_3 in the first stage and then cordination with propeyl linker in the final steps with DABCO dobel head ionic tags, the shape of Fe_2O_3@$SiO_2(CH_2)_3$-Cl[DABCO-NO_2]C(NO_2)$_3$ were seperated, arranged and improved to a symmetrical doble spherical MNPs. As shown in Figure 5b, the crystal Fe_2O_3-MNPs distance layer of final nanoparticles of catalyst are around 0.26 nm which has good correlation with the plane layer (311) in sharpest peak at the powder XRD results. Moreover, the FESEM results clearly aproved the spherical uniform of the MNPs in the sample (**Figure 5c**).

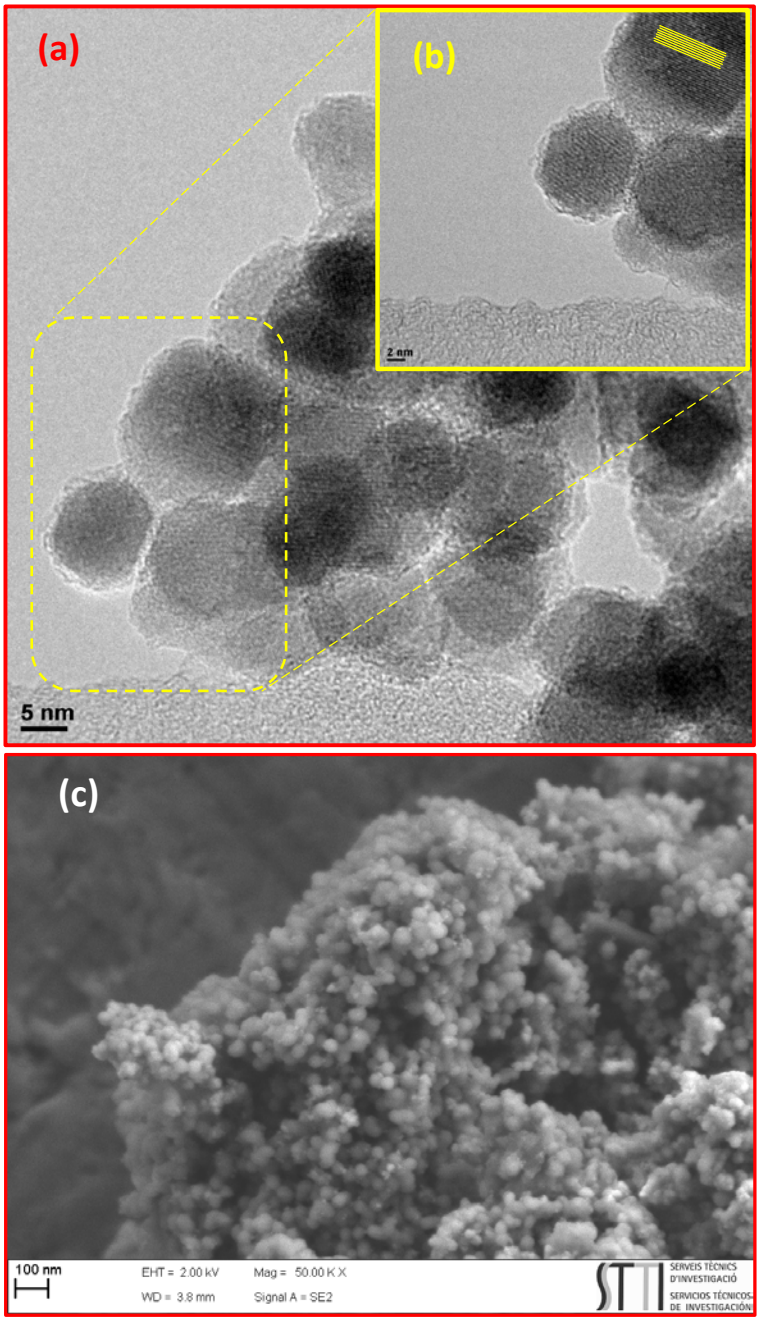

Figure 5. a) High resolution transmission electron microscopy (HRTEM) images of a) Fe_2O_3@$SiO_2(CH_2)_3$-Cl[DABCO-NO_2]C(NO_2)$_3$ in 5nm scale; inlet: b) 2nm selected scale area (**V**); and c) field emission scanning electron microscopy (FESEM) of final catalyst nanoparticles in 100nm scale.

Thermogravimetric (TG) analysis, derivatives thermal gravimetric analysis (DTG), and the differential thermal analysis (DSC) were performed to analyze the content of DABCO ionic tags in catalysts under argon atmosphere (**Figure 6**). From the performed studies, it may be inferred that the two main weight loss upon heating, first, from ambient temperature to 110 ºC with weight loss of ~ 1 wt% could be related to the removal of surface-adsorbed water and organic solvents applied during the catalyst preparation and the second part from 200 ºC to 300 ºC with weight loss of >11 wt% could be reasoned for the ionic molten salt nature of DABCO with diferrent NO_2 parts. Moreover, from analysis diagram from the results of DSC in figure 6b, the catalysts has shown three different thermal behaveriuos. in the firs stage, it has shown downward and exotemic pattern from 25 ºC to 110 ºC, in the second and main part of catalyst, from 110 ºC to ~ 400 ºC it has shown a upwards with endothrmic pattern and finally, in the last part from ~ 400 ºC to 800 ºC it has shown again a downward behaviour with endothermic maner.

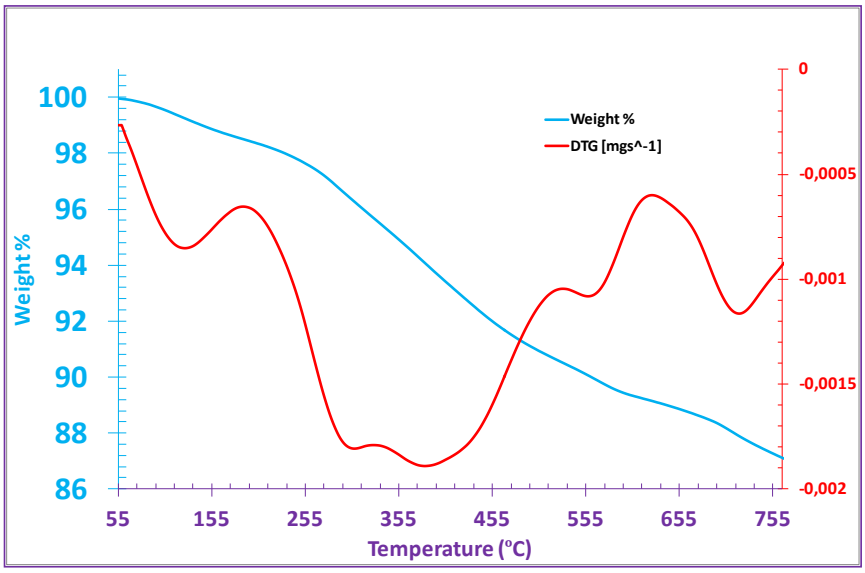

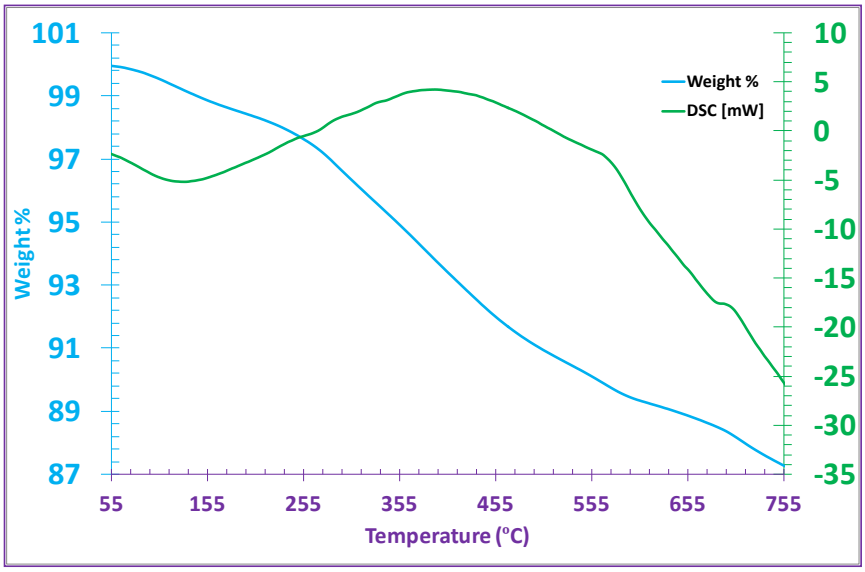

Figure 6. a) Thermal gravimetric analysis (TG/DTG), and b) (TGA/DSC) of MNPs.

Further observations were made by Powder X-ray diffraction (XRD) to illustrate the crystalline structure of MNPs in a range of $10 < 2\theta < 90°$ (**Figure 7**). The upward typical iron oxide spectrum pattern was showed peaks at 2θ values of 14.96°, 18.38°, 30.24°, 35.63°, 43.28°, 53.73°, 57.27°, 62.93° and 74.47° related to (110), (111), (220) (311), (400), (422), (511), (440) and (533) corresponding to planes of iron oxide (Fe_xO_y). Moreover, as clear from the Maghemite (Fe_2O_3) with blue standard lines (JCP2: 00-039-1346) and magnetie (Fe_3O_4) with red standard lines (JCP2: 01-075-1609) as the standard references, the center of each peaks may be adjusted with maghemite (Fe_2O_3) structures more than magnetie (Fe_3O_4). Also the sharpest peak in XRD spectrum of the catalyst has been correlated to plane (311) at 30.24º with 2.51Å layer distance and the largest layer distance are connected to layer (220) at 30.24º with 2.95 Å.

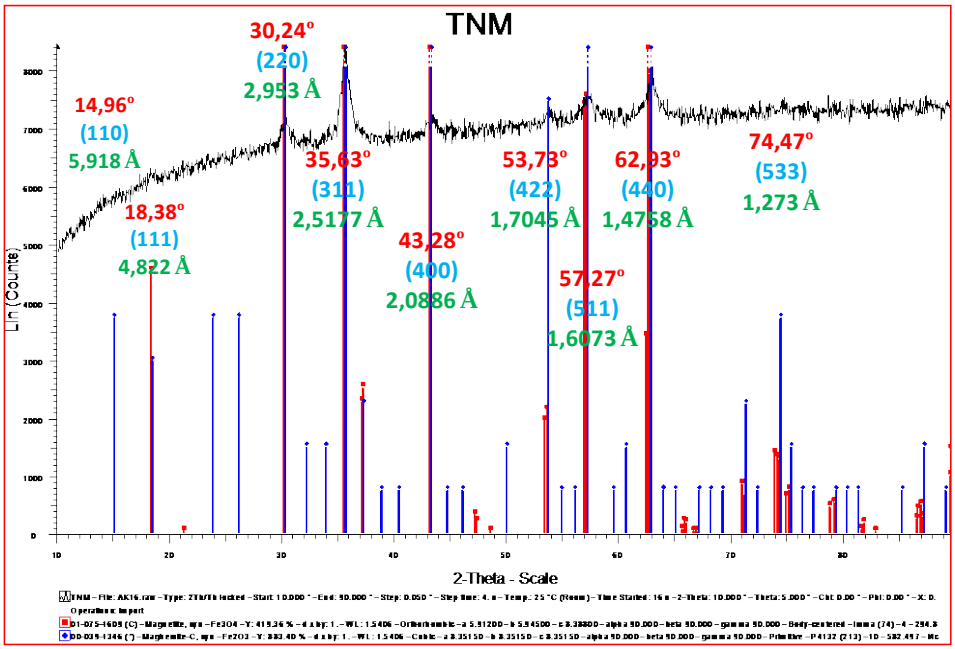

Figure 7. powder XRD pattern of MNPs, inlet blue solid lines: JCP2: 00-039-1346 for standard data base of Fe_2O_3 and inlet red solid lines: (JCP2: 01-075-1609) for standard data base of Fe_3O_4

In continuation investigation of catalyst, N_2 adsorption/desorption isotherm was performed to characterize the porosity and total surface area of the magnetic nanoparticles. As shown in **Figure 8a**, catalyst exhibited type II isotherm according to the IUPAC definition and with H_3 type hysteresis loop, which displaied the presence of a nanoporous structure. The surface area and pore volume of the catalyst are listed in **Table 2**. The determined Brunauer-Emmett-Teller (BET), BJH and DR specific surface areas of Fe_2O_3@$SiO_2(CH_2)_3$-Cl[DABCO-NO_2]$C(NO_2)_3$ are 112.766, 61.676 and 108.923 m^2g^{-1} respectively. Moreover, the total pore volume was achived 0.31 cm^3g^{-1}. the corresponding pore-size distribution (PSD) of nanopores (inset of Figures 10b) was calculated from the adsorption branch on the basis of BJH model (Figure 8b) and is centered at 15 nm, according to the (BJH) model.

[Comentario U1]: دکتر خشنود عزیز
با سلام: این قسمت را نمی فهمم لطفا طبق تشخیص خودتان اصلاح فرمائید.

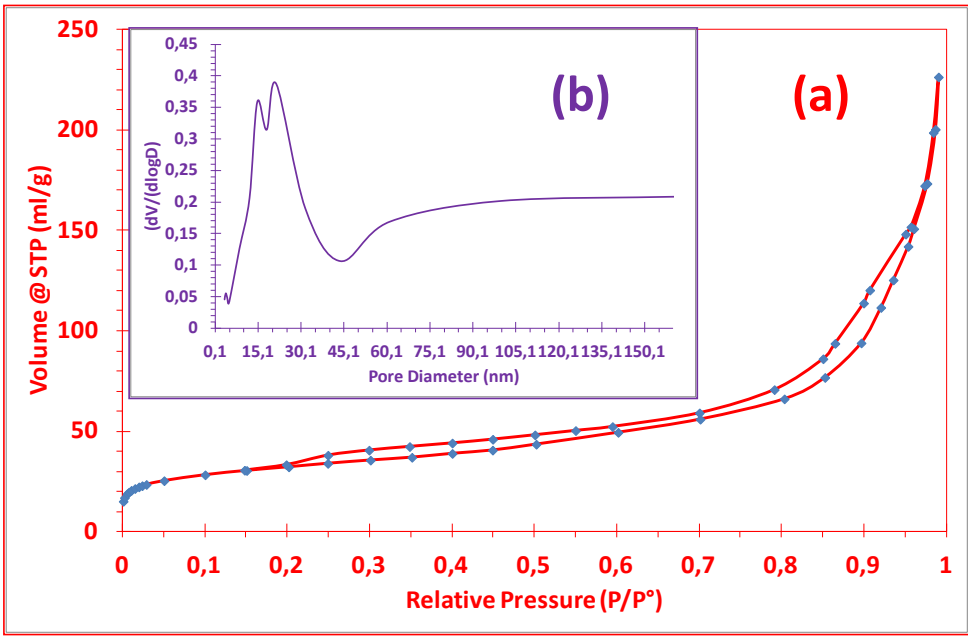

Figure 8 a) Nitrogen adsorption/desorption isotherms and b) inset: BJH pore size distribution of Fe_2O_3@$SiO_2(CH_2)_3$-Cl[DABCO-NO_2]C(NO_2)$_3$

Table 1. Textural properties of Fe_2O_3@$SiO_2(CH_2)_3$-Cl[DABCO-NO_2]C(NO_2)$_3$

S_{BET}[a] (m^2g^{-1})	S_{BJH}[b] (m^2g^{-1})	S_m[c] (m^2g^{-1})	V_t[d] (cm^3g^{-1})	pore size[e] (nm)
112.766	61.676	108.923	0.31	14.826

[a] S_{BET}: total surface area. [b] S_{BJH}: surface area estimated by BJH model applied to the desorption branch of the isotherm. [c] S_m: Micropore surface area estimated by DR model. [d] V_t: total pore volume. [e] Obtained from BJH.

The magnetic measurement of Fe_2O_3@$SiO_2(CH_2)_3$-Cl[DABCO-NO_2]C(NO_2)$_3$ was also studied. Its VSM was compared with its precursors Fe_2O_3, Fe_2O_3@SiO_2 and Fe_2O_3@$SiO_2(CH_2)_3$Cl. As shown in **Figure 9**, after adding of each layer, the saturation

magnetization reduces from 70.55 emu g^{-1} for Fe_2O_3 to 50.01 emu g^{-1} for describe $Fe_2O_3@SiO_2(CH_2)_3$-Cl[DABCO-NO_2]C$(NO_2)_3$.

[U2 Comentario]: دکتر خشنود عزیز
لطفا این بخش را لطفا ادیت فرمائید.

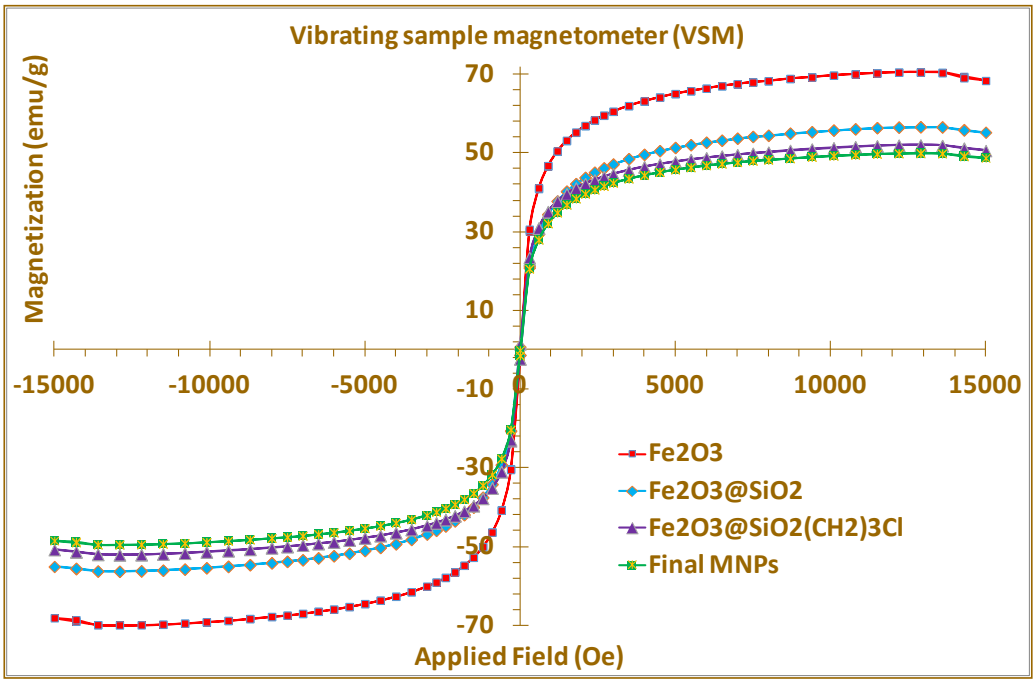

Figure 9. VSM magnetization curves of catalyst was compared with its precursors Fe_2O_3, $Fe_2O_3@SiO_2$, $Fe_2O_3@SiO_2(CH_2)_3Cl$, nano particles

After fully Characterization and investigation of $Fe_2O_3@SiO_2(CH_2)_3$-Cl[DABCO-NO_2]C$(NO_2)_3$ structure, it was used as nano magnetic catalyst in the condensation reaction of 3-methyl-1-phenyl-1*H*-pyrazol-5-amine, malnonitrile and various aromatic aldehydes for the synthesis of pyrazolo[3,4-*b*]-pyridine derivatives. For this aim, at first to optimize the reaction conditions, the reaction of benzaldehyde, 3-methyl-1-phenyl-1*H*-pyrazol-5-amine and malononitrile was selected as model reaction. The results for the optimization of temperatures, catalyst amount and solvents are summarized in **Table 2**. As shown in Table 2, the best results for the synthesis of pyrazolo[3,4-*b*]-pyridines were achieved when the reaction curried out at 100

°C in the presence of 5 mg $Fe_2O_3@SiO_2(CH_2)_3$-Cl[DABCO-NO_2]C(NO_2)$_3$ under solvent free conditions.

Table 2. The reaction of benzaldehyde, 3-methyl-1-phenyl-1*H*-pyrazol-5-amine and malononitrile under different conditions.[a]

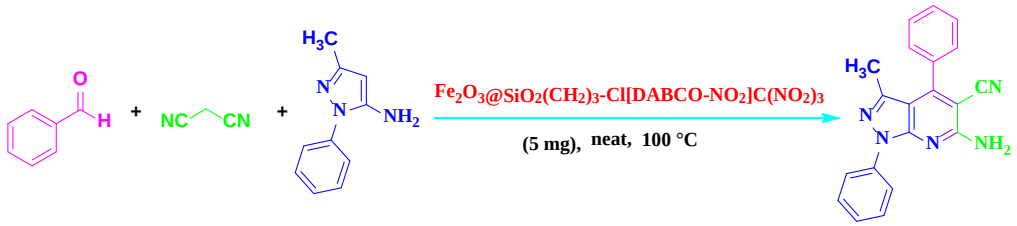

Entry	Solvent	Load of Catalyst (mg)	Temp. (°C)	Time (min)	Yield (%)[b]
1	-	10	80	30	81
2	-	10	100	25	89
3	-	10	110	25	89
4	-	8	100	25	89
5	**-**	**5**	**100**	**25**	**89**
6	-	3	100	40	75
7	EtOH	5	Reflux	240	35
8	EtOAc	5	Reflux	180	32
9	H_2O	5	Reflux	240	Trace
10	CH_3CN	5	Reflux	180	38

[a]Reaction conditions: aryl aldehyde (1 mmol), malononitrile (1.2 mmol, 79 mg), 3-methyl-1-phenyl-1H-pyrazol-5-amine (1 mmol, 173 mg) and [$Fe_2O_3@SiO_2(CH_2)_3$-Cl[DABCO-NO_2]C(NO_2)$_3$] (5 mg). [b]Isolated yield.

After optimizing the reaction conditions, to assess the scope and limitations of the catalyst, 3-methyl-1-phenyl-1*H*-pyrazol-5-amine was reacted with various aromatic aldehydes (bearing electron releasing and electron-withdrawing groups) and malononitrile. As shown in **Table 3**, the results indicate that this method is appropriate for the synthesis of pyrazolo[3,4-*b*]-pyridine derivatives.

Table 3. Synthesis of pyrazolo[3,4-*b*]-pyridine derivatives using $Fe_2O_3@SiO_2(CH_2)_3$-Cl[DABCO-NO_2]C(NO_2)$_3$ as a new nanomagnetic catalyst under solvent free conditions.[a]

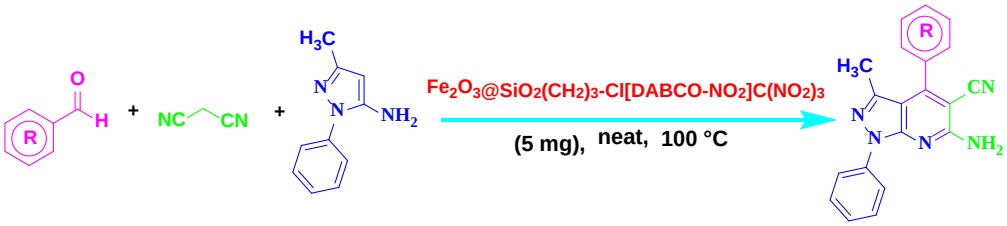

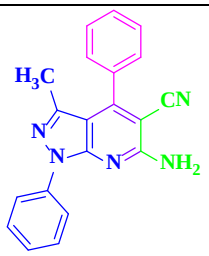

(1a)

time: 25 min; yield: 89%;

Mp: 210-212 °C [23]

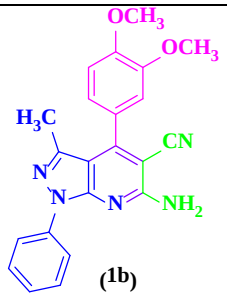

(1b)

time: 35 min; yield: 92%;

Mp: 218-220 °C [20]

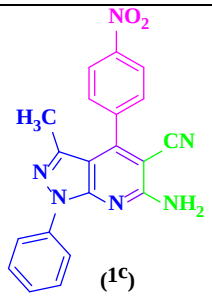

(1c)

time: 20 min; yield: 90%;

Mp: 223-225 °C [23]

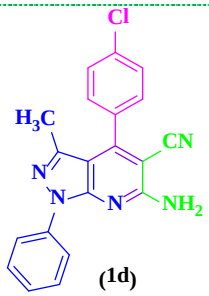

(1d)

time: 20 min; yield: 91%;

Mp: 194-198 °C [20]

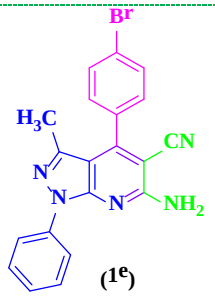

(1e)

time: 25 min; yield: 92%;

Mp: 216-217 °C [23]

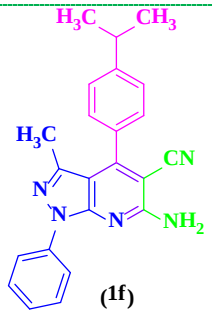

(1f)

time: 35 min; yield: 87%;

Mp: 198-200 °C

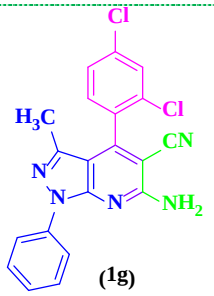

(**1g**)

time: 30 min; yield: 91%;

Mp: 167-169 °C

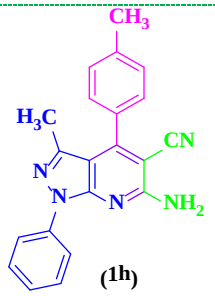

(**1h**)

time: 30 min; yield: 93%;

Mp: 200-202°C [20]

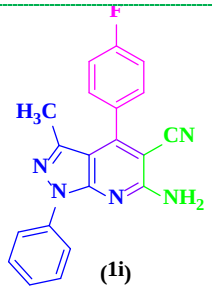

(**1i**)

time: 20 min; yield: 88%;

Mp: 214-216 °C [20]

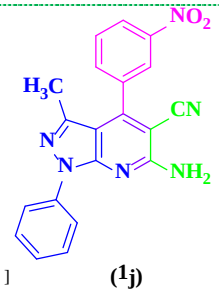

(**1j**)

time: 20 min; yield: 85%;

Mp: 157-159°C [23]

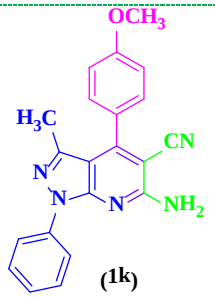

(**1k**)

time: 25 min; yield: 91%;

Mp: 195-197 °C [20]

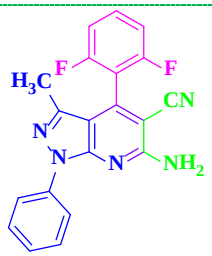

(**1l**)

time: 35 min; yield: 85%;

Mp: 227-229 °C

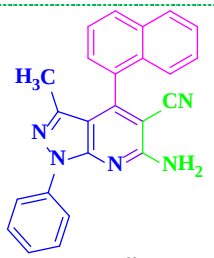

(**1m**)

time: 35 min; yield: 85%;

Mp: 195-197 °C

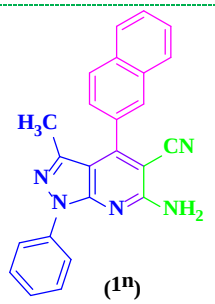

(**1n**)

time: 30 min; yield: 90%;

Mp: 270-272 °C

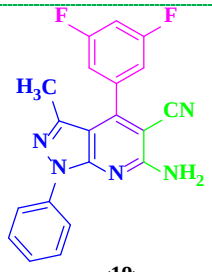

(**1o**)

time: 25 min; yield: 87%;

Mp: 198-200 °C

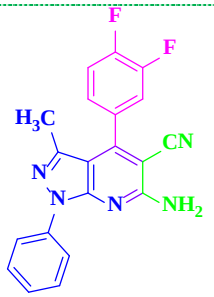 **(1p)**	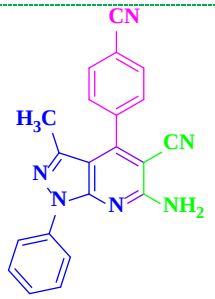 **(1q)**
time: 25 min; yield: 89%; Mp: 203-205 °C	time: 25 min; yield: 93%; Mp: 237-239 °C

[a]Reaction conditions: aryl aldehyde (1 mmol), malononitrile (1.2 mmol, 79 mg), 3-methyl-1-phenyl-1H-pyrazol-5-amine (1 mmol, 173 mg) and $[Fe_2O_3@SiO_2(CH_2)_3\text{-}Cl[DABCO\text{-}NO_2]C(NO_2)_3]$ (5 mg). [b] All yields are isolated yields.

The recovery and reusing of $Fe_2O_3@SiO_2(CH_2)_3\text{-}Cl[DABCO\text{-}NO_2]C(NO_2)_3$ were investigated under optimized conditions for the reaction of benzaldehyde, 3-methyl-1-phenyl-1*H*-pyrazol-5-amine and malononitrile. In these conditions, the nano magnetic catalyst was reused up to nine times with only a marginal decrease in its reactivity. After each use, in order to separation of the catalyst, the reaction mixture was dissolved in acetone. Then, the catalyst was extracted by using an external magnet and reused in the subsequent reactions after washing. As shown in **Figure 10**, activity of this catalyst is maintained up to nine times without any significant changes in the yields and reaction times.

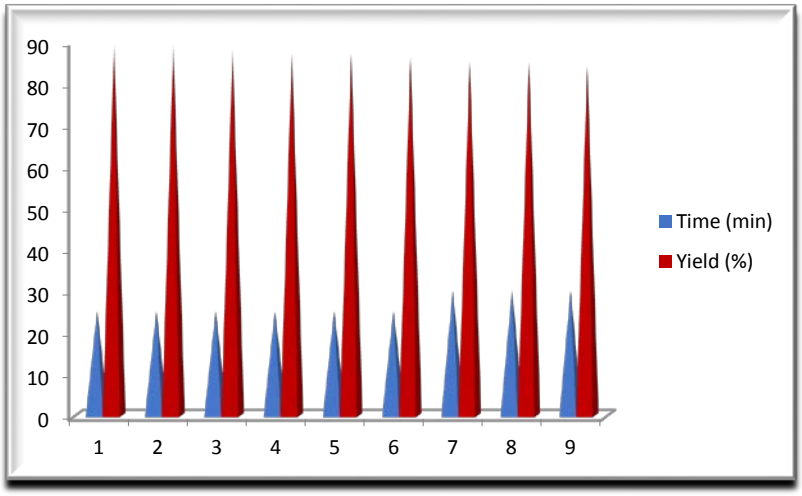

Figure 10. the reaction of benzaldehyde, 3-methyl-1-phenyl-1*H*-pyrazol-5-amine and malononitrile using recycled nano magnetic catalyst.

According to previously reported methods [20,23], an applicable mechanism for the synthesis of pyrazolo[3,4-*b*]-pyridines is proposed. In the beginning, malononitrile reacts with aldehyde which is activated by Fe_2O_3@$SiO_2(CH_2)_3$-Cl[DABCO-NO_2]C(NO_2)$_3$ to affords cyanoolefin **2** by removing one molecule of HNO_3 [28]. Then, 3-methyl-1-phenyl-1*H*-pyrazol-5-amine attacks to the intermediate **2** as a Michael acceptor to gives **3**. Next, cyclization of **3** creates intermediate **4** which is converting to desired product via hyperconjugative-like anomeric based oxidation (**Scheme 3**). Previously reported studied have proposed an aerobic oxidation of intermediate **5** to target molecule **7**. In contrast to the previously reported mechanistic route [23] for the final step of the aforementioned described organic synthesis, we suggested that, this step might be proceeded via unusual hydride transfer as well as Cannizzaro reaction (**Scheme 4**) [29] pyranose acatals (**Scheme 5**) [30] and H_2 releasing from tricyclic orthoamide (**Scheme 6**) [31]**.** As presented in **Scheme 7**, isomer with equatorial 2-methoxy group is more reactive than its axial isomer due to two lone pair anomeric assistance to the departure of the hydride leaving group.[30]

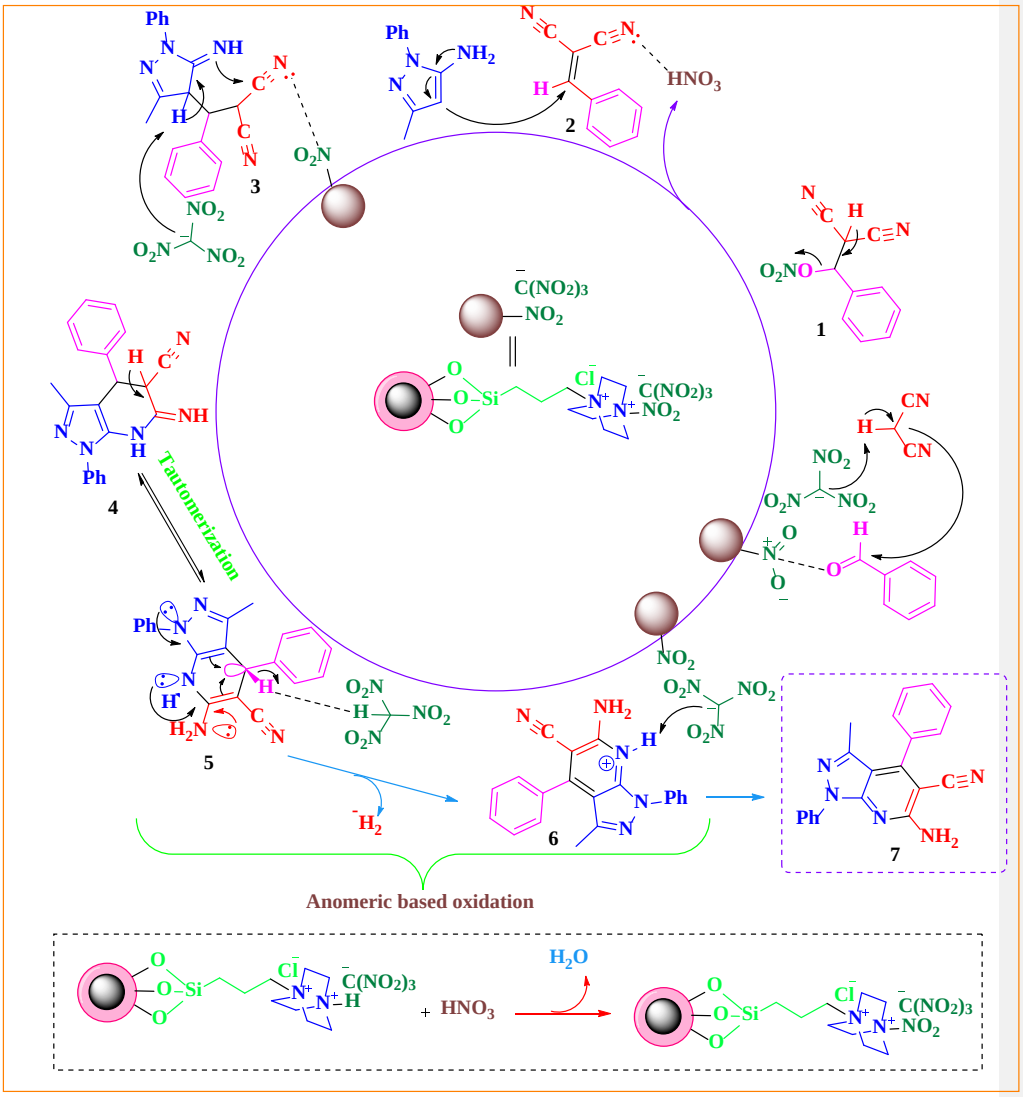

Scheme 3. The proposed mechanism for the synthesis of pyrazolo[3,4-*b*]-pyridines in the presence of Fe_2O_3@$SiO_2(CH_2)_3$-Cl[DABCO-NO_2]$C(NO_2)_3$

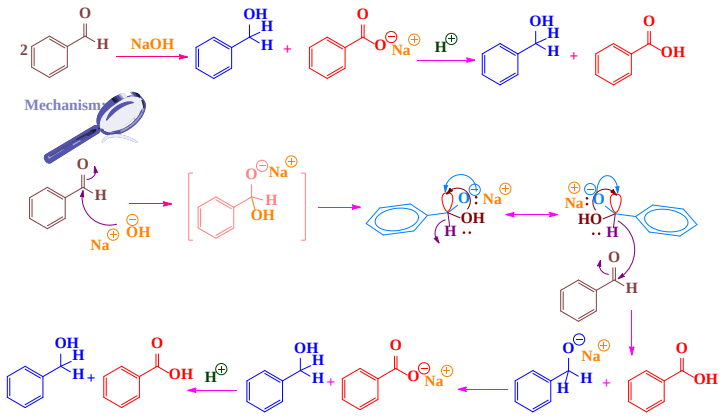

Scheme 4. The suggested mechanism for the in-situ oxidation-reduction in Cannizzaro reaction by uncommon hydride transfer *via* ABO mechanism.[29]

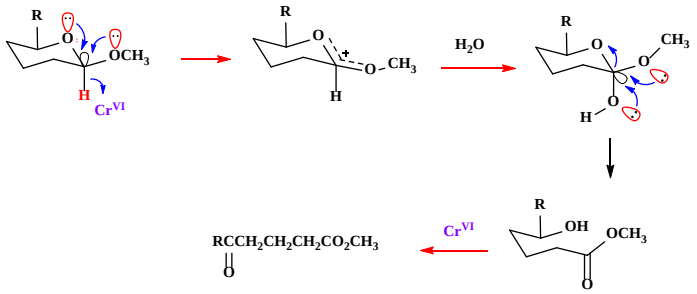

Scheme 5. An excellent example which had been reported for an unusual hydride transfer from 2-methoxypyranose by ABO mechanism.[30]

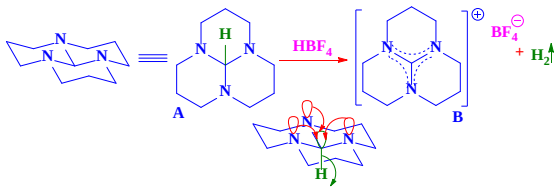

Scheme 6. A striking example which had been detected for an unusual hydride transfer from tricyclic orthoamide (A) by ABO mechanism. [31]

Two lone pair orbitals in antiperiplanar arrangement **Only one lone pair orbital in antiperiplanar arrangement**

Scheme 7. Isomer with equatorial 2-methoxy group is more reactive than its axial isomer due to two lone pair anomeric assistance to the departure of the hydride leaving group [30].

As above mentioned, we have introduced an "anomeric based oxidation (ABO)" terminology for the final step in mechanistic route in the synthesis of various molecules such as: 1,4-dihydropyrano-[2,3-*c*]-pyrazoles [32], 2,4,6-triarylpyridines [33], 2-amino-3-cyanopyridines [34], 2-sbstituted benz-(imida, oxa and othia)-zole derivatives [28], oxidative aromatization of pyrazolines and 1,4-dihydropyridines [35], sulfanylpyridines [36], and 2-amino-4-aryl-6-(arylamino)pyridine-3,5-dicarbonitriles [37]. For approving the aforementioned idea, reaction was carried out under both nitrogen and argon atmosphere and in the absence of any molecular oxygen. It was found that, the reaction progressed under atmosphere of nitrogen and argon slightly slower than normal reaction condition (air atmosphere). On the basis of the above-mentioned evidence, conversion of intermediate **3** to target molecule **4** might be occurred by unusual hydride transfer and releasing of molecular hydrogen (H_2). The C–H bond is weakened *via* hyper conjugation-like of the nitrogen lone pairs into the anti-bonding of C-H ($\sigma^*_{C\text{-}H}$ orbital) which can be broken by reaction with a proton to give molecular hydrogen.

Conclusions

In summary, magnetic nanoparticles (MNPs) surface were chemically modified with $Cl[DABCO\text{-}NO_2]C(NO_2)_3$ tags and $Fe_2O_3@SiO_2(CH_2)_3\text{-}Cl[DABCO\text{-}NO_2]C(NO_2)_3$ was designed, synthesized and fully characterized by several techniques such as FT-IR, EDX/mapping, FESEM, HRTEM, TGA, DTG, DSC, powder XRD, N_2 adsorption (BET) and

VSM. The described nano magnetic particle was used as an efficient catalyst for the three-component condensation reaction of aryl aldehydes, 3-methyl-1-phenyl-1*H*-pyrazol-5-amine and malononitrile under solvent free conditions. Short reaction times, good yields and easy work-up, reusability of catalyst, and solvent free condition are major advantages of this work. Also, in the possible mechanism, an anomeric based oxidation was suggested for the final step of pyrazolo[3,4-*b*]-pyridines synthesis.

Experimental

In continuation of our researches on the exploring of new nano magnetic catalysts [38], herein, we designed and synthesized the nano magnetic particles named Fe_2O_3@$SiO_2(CH_2)_3$-Cl[DABCO-NO_2]$C(NO_2)_3$. The mentioned nano particles were applied as an efficient and reusable catalyst in the synthesis of pyrazolo[3,4-*b*]-pyridines via anomeric based oxidation under solvent free conditions.

General

All chemicals were obtained from Merck, Sigma Aldrich and used without further purification. The known products have been identified by comparison of their melting points and spectral data with those reported in the literature. Progress of the reactions was monitored by TLC using silica gel SIL G/UV 254 plates. Melting points were recorded on a Büchi B-545 apparatus in open capillary tubes. R_f values were measured using EtOAc: *n*-Hexane (3:7) as elution solvents. Fourier transformed infrared (FTIR) spectra of the catalyst and the synthesized products were performed on a FTIR spectrometer Perkin-Elmer spectrum 65 using KBr disks. High resolution mass spectra (GC/QTOF, Chemical Ionization (CI) mode with 20% CH_4 and 300 °C source temperature) were obtained using an Agilent 7200 Network spectrometer. Each sample was dissolved in $CHCl_3$ and directly injected to the instrument by using standard Agilent glass capillary. ^{1}H NMR (300 and 400 MHz) spectra were obtained on a Bruker Avance 300 and a

Bruker Avance 400 NMR spectrometers under proton coupled mode using $CDCl_3$ as solvent. ^{13}C NMR (75, 101 and 126 MHz) spectra were acquired on a Bruker Avance 300, a Bruker Avance 400 NMR and Bruker Avance DRX 500 NMR spectrometer in the proton decoupled mode at 20 °C in $CDCl_3$ as solvent. Chemical shifts are given in δ (parts per million) and the coupling constants (*J*) in Hertz. ^{19}F NMR (282 and 376 MHz) spectra were recorded on a Bruker Avance 300 and a Bruker Avance 400 NMR spectrometer, in proton coupled mode. Data for ^{1}H NMR spectra is reported as follows: chemical shift (ppm), multiplicity (s, singlet; d, doublet; t, triplet; q, quartet; m, multiplet; and br., broad), coupling constant (Hz), and integration. Simultaneous thermal gravimetry analysis TG-DSC, were carried out on a Mettler Toledo equipment (model TGA/SDTA851and/LF/1600), capable of working between room temperature and 1600 °C under inert Argon atmosphere and is equipped with a 34 position autosampler. The experiment was carried out at 25°C and using a heating rate of 25 °C min^{-1} up to 800 °C. Powder X-ray diffraction (XRD) pattern was recorded with a Bruker D8-Advance with mirror Goebel (non-planar samples), high temperature Chamber (up to 900°C), generator of x-ray KRISTALLOFLEX K 760-80F (power: 3000W, voltage: 20-60KV and current: 5-80 mA) and with a tube of RX with copper anode Kα (λ = 0.154 nm) in the range $10° < 2\theta < 90°$. Physical adsorption and physisorption of N_2 isotherms were measured at 77 K with an AUTOSORB-iQ-XR-2 analyzer. The catalyst was degasses before the experiment for one day at 100 °C under high vacuum condition. The Brunauer-Emmett-Teller (BET) method was used to calculate the specific surface areas (S_{BET}). By using the Barrett-Joyner-Halenda (BJH) model, the pore volumes and pore size distributions were derived from the adsorption branches of isotherms. The micropore surface area (S_{BET} micro) was calculated using the *V-t* plot method. Scanning electron microscopy (SEM) studies were performed using a Hitachi S3000N, equipped with an X-ray detector Bruker XFlash 3001 for microanalysis (EDX) and elemental mapping. Field emission scanning electron microscopy (FESEM) studies were performed using a Merlin VP Compact

from Zeiss, equipped with an EDS microanalysis system Quantax 400 from Bruker. The resolution is 0.8 nm at 15 kV and 1.6 nm at 1 kV. Field emission equipment is able to work at voltages very reduced (from 0.02 kV to 30 kV) allowing to observe beam sensitive samples without damaging them and minimizing the charging effects. High-resolution transmission electron microscopy (HRTEM) images were obtained using a JEOL JEM-2010 microscope operating at an accelerating voltage of 200 kv. This microscope is equipped with an X-ray detector OXFORD INCA Energy TEM 100 for microanalysis (EDS) and acquisition of the images is made by means of a digital camera GATAN ORIUS SC600 mounted on-axis, integrated with the program GATAN DigitalMicrograph 1.80.70 for GMS 1.8.0. Sample was prepared by drop casting the dispersed particles in absolute ethanol onto a 300-mesh copper grid from TED PELLA, INC. model 01883-F, coated with a lacey formvar film enforced by a heavy coating of carbon. Holes are completely open. The magnetic behavior of the nano magnetic catalyst was also measured by a vibrating sample magnetometer (VSM) instrument from Meghnatis Daghigh Kavir Company model LBKFB.

General procedure for the preparation of the novel nanomagnetic catalyst

Fe_2O_3 nanoparticles were prepared according to the previously reported procedure. Then, 1 g of Fe_2O_3 nanoparticles (**I**) was dispersed in toluene. In the next step, to coat the surface of the Fe_2O_3 with SiO_2, 1.5 mL tetraethyl orthosilicate (TEOS) was added drop-wise and the reaction was continued for 12 h under reflux conditions. The resultant Fe_2O_3@SiO_2 (**II**) was washed with ethanol for three times and dried. After that, in order to silanate the silica coated nanomagnetic particles, 3-chloropropyltrimethoxysilane (1.5 mL) was added to the mixture in toluene under reflux conditions to give (**III**). After 12 h, compound (**III**) was washed with ethanol, then 1,4-diazabicyclo[2.2.2]octane (DABCO) (6 mmol, 0.67 g) was added and refluxed in ethanol for 12 h to afford compound (**IV**). Eventually, tetranitromethane (6 mmol, 1.18 g, 0.73 mL) was added

to compound (**IV**) in toluene under reflux conditions to give (**V**) as a novel nano magnetic catalyst (**Scheme 2**).

General procedure for the synthesis of pyrazolo[3,4-*b*]-pyridine derivatives

To a round-bottom flask containing a mixture of aldehydes (1mmol), 3-methyl-1-phenyl-1*H*-pyrazol-5-amine (1 mmol, 173 mg) and malnonitrile (1.2 mmol, 79 mg) 5 mg Fe_2O_3@$SiO_2(CH_2)_3$-Cl[DABCO-NO_2]C(NO_2)$_3$ was added. The resulting mixture was stirred magnetically under solvent-free conditions at 100 °C. After completion of the reaction which was monitored by TLC, the mixture was cooled to room temperature. Then, acetone was added to separate the catalyst by an external magnet. After evaporation of the solvent, the resulting solid was recrystallized in ethanol to give pure products. Finally, the nanomagnetic catalyst was reused for the next run (**Scheme 1**).

Results spectral data of products:

6-amino-3-methyl-1,4-diphenyl-1H-pyrazolo[3,4-b]pyridine-5-carbonitrile (1a):

Isolated as white solid, (290 mg, 89%), R_f: 0.52, Melting point: 210 – 212 °C; FT-IR: υ (cm^{-1}) = 3366, 3219, 2217, 1626, 756; ^{1}H NMR (300 MHz) δ 8.11 (dd, *J* = 8.6, 1.1 Hz, 2H), 7.66 – 7.39 (m, 7H), 7.35 – 7.27 (m, 1H), 5.42 (br. s, 2H), 2.03 (s, 3H). ^{13}C NMR (101 MHz) δ 158.3, 152.8, 150.9, 144.4, 138.8, 134.0, 129.9, 129.0, 128.6 (2c), 126.2, 121.5, 116.8, 109.5, 88.5, 14.7; HRMS calcd. for $C_{20}H_{15}N_5$ [M^+] 325.1327, found. 325.1343.

6-amino-4-(3,4-dimethoxyphenyl)-3-methyl-1-phenyl-1H-pyrazolo[3,4-b]pyridine-5-carbonitrile (1b)

Isolated as white solid, (354 mg, 92%), R_f: 0.35, Melting point: 218 – 220 °C; FT-IR: υ (cm^{-1}) = 3332, 3222, 2210, 1626, 765; ^{1}H NMR (300 MHz) δ 8.10 (dd, *J* = 8.6, 1.1 Hz, 2H), 7.58 – 7.42

(m, 2H), 7.35 – 7.27 (m, 1H), 7.11 – 7.00 (m, 2H), 6.98 (d, *J* = 1.5 Hz, 1H), 5.41 (br. s, 2H), 3.98 (s, 3H), 3.94 (s, 3H), 2.13 (s, 3H). ^{13}C NMR (101 MHz) δ 158.4, 152.7, 150.9, 150.3, 148.8, 144.4, 138.8, 129.0, 126.2 (2C), 121.7, 121.5, 117.1, 111.9, 111.0, 109.6, 88.6, 56.1, 56.0, 15.0; HRMS calcd. for $C_{22}H_{19}N_5O_2$ [M^+] 385.1539, found. 385.1557.

6-amino-3-methyl-4-(4-nitrophenyl)-1-phenyl-1H-pyrazolo[3,4-b]pyridine-5-carbonitrile (1c):

Isolated as pale yellow solid, (333 mg, 90%), R_f: 0.60, Melting point: 223 – 225 °C; FT-IR: υ (cm^{-1}) = 3350, 3208, 2214, 1619, 1581, 1348, 769; ^{1}H NMR (300 MHz) δ 8.53 – 8.34 (m, 2H), 8.10 (d, *J* = 7.7 Hz, 2H), 7.79 – 7.59 (m, 2H), 7.51 (t, *J* = 7.9 Hz, 2), 7.33 (t, *J* = 7.4 Hz, 1H), 5.47 (br. s, 2H), 2.03 (s, 3H). ^{13}C NMR (101 MHz) δ 158.1, 150.8, 149.7, 148.8, 143.6, 140.4, 138.5, 129.9, 129.0, 126.4, 124.0, 121.5, 116.1, 109.0, 88.0, 14.8; HRMS calcd. for $C_{20}H_{14}N_6O_2$ [M^+] 370.1178, found. 370.1187.

6-amino-4-(4-chlorophenyl)-3-methyl-1-phenyl-1H-pyrazolo[3,4-b]pyridine-5-carbonitrile (1d):

Isolated as white solid, (327 mg, 91%), R_f: 0.74, Melting point: 194 – 198 °C; FT-IR: υ (cm^{-1}) = 3308, 3187, 2214, 1633, 824; ^{1}H NMR (300 MHz) δ 8.10 (dd, *J* = 8.5, 1.0 Hz, 2H), 7.61 – 7.45 (m, 4H), 7.45 – 7.38 (m, 2H), 7.31 (t, *J* = 7.4 Hz, 1H), 5.43 (br. s, 12H), 2.06 (s, 3H). ^{13}C NMR (101 MHz) δ 158.3, 151.3, 150.9, 144.1, 138.7, 136.3, 132.4, 130.0, 129.0 (2C), 126.3, 121.5, 116.6, 109.4, 88.4, 14.8; HRMS calcd. for $C_{20}H_{14}ClN_6$ [M^+] 359.0938, found. 370.0951.

6-amino-4-(4-bromophenyl)-3-methyl-1-phenyl-1H-pyrazolo[3,4-b]pyridine-5-carbonitrile (1e):

Isolated as white solid, (372 mg, 92%), R_f: 0.77, Melting point: 216 – 217 °C; FT-IR: υ (cm^{-1}) = 3369, 2920, 2217, 1637, 760; ^{1}H NMR (300 MHz) δ 8.10 (dd, *J* = 8.6, 1.1 Hz, 2H), 7.75 – 7.67 (m, 2H), 7.54 – 7.45 (m, 2H), 7.38 – 7.28 (m, 3H), 5.43 (br. s, 2H), 2.06 (s, 3H). ^{13}C NMR (101

MHz) δ 158.3, 151.3, 150.9, 144.1, 138.7, 132.8, 132.0, 130.2, 129.0, 126.3, 124.5, 121.5, 116.6, 109.3, 88.3, 14.8; HRMS calcd. for $C_{20}H_{14}BrN_5$ [M^+] 403.0433, found. 403.0437.

6-amino-4-(4-isopropylphenyl)-3-methyl-1-phenyl-1H-pyrazolo[3,4-b]pyridine-5-carbonitrile (1f):

Isolated as white solid, (320 mg, 87%), R_f: 0.71, Melting point: 198 – 200 °C; FT-IR: υ (cm^{-1}) = 3308, 3190, 2211, 1635, 709; ^{1}H NMR (300 MHz) δ 8.11 (dd, *J* = 8.6, 1.1 Hz, 12H), 7.53 – 7.45 (m, 2H), 7.40 (br. s, 4H), 7.34 – 7.27 (m, 1H), 5.42 (br. s, 2H), 3.10 – 2.93 (m, 1H), 2.06 (s, 3H), 1.34 (s, 3H), 1.32 (s, 3H). ^{13}C NMR (101 MHz) δ 158.4, 153.1, 150.9, 144.657, 138.8, 131.2, 129.0, 128.7, 126.6, 126.1, 121.5, 117.1, 109.6, 88.5, 34.0, 23.9, 14.8; HRMS calcd. for $C_{23}H_{21}N_5$ [M^+] 367.1797, found. 367.1812.

6-amino-4-(2,4-dichlorophenyl)-3-methyl-1-phenyl-1H-pyrazolo[3,4-b]pyridine-5-carbonitrile (1g):

Isolated as white solid, (359 mg, 91%), R_f: 0.82, Melting point: 167 – 169 °C; FT-IR: υ (cm^{-1}) = 3350, 3213, 2214, 1614, 757; ^{1}H NMR (300 MHz) δ 8.11 (dd, *J* = 8.7, 1.1 Hz, 2H), 7.63 (d, *J* = 2.0 Hz, 1H), 7.55 – 7.42 (m, 3H), 7.35 – 7.27 (m, 2H), 5.45 (br. s, 2H), 2.02 (s, 3H). ^{13}C NMR (101 MHz) δ 158.2, 150.8, 148.2, 144.1, 138.7, 136.7, 133.5, 131.7, 130.8, 130.1, 129.0, 127.7, 126.3, 121.5, 115.9, 109.6, 88.8, 13.5; HRMS calcd. for $C_{20}H_{13}Cl_2N_5$ [M^+] 393.0548, found. 393.0564.

6-amino-3-methyl-1-phenyl-4-(p-tolyl)-1H-pyrazolo[3,4-b]pyridine-5-carbonitrile (1h):

Isolated as white solid, (315 mg, 93%), R_f: 0.72, Melting point: 200 – 202 °C; FT-IR: υ (cm^{-1}) = 3325, 3216, 2211, 1629, 762; ^{1}H NMR (300 MHz) δ 8.16 – 8.07 (m, 2H), 7.54 – 7.44 (m, 2H), 7.36 (br. s, 4H), 7.33 – 7.27 (m, 1H), 5.39 (br. s, 2H), 2.47 (s, 3H), 2.07 (s, 3H). ^{13}C NMR (101 MHz) δ 158.4, 153.1, 150.9, 144.5, 140.0, 138.8, 131.0, 129.3, 129.0, 128.5, 126.2, 121.6, 117.0, 109.5, 88.5, 21.5, 14.8; HRMS calcd. for $C_{21}H_{17}N_5$ [M^+] 339.1484, found. 339.1495.

6-amino-4-(4-fluorophenyl)-3-methyl-1-phenyl-1H-pyrazolo[3,4-b]pyridine-5-carbonitrile (1i):

Isolated as white solid, (302 mg, 88%), R_f: 0.61, Melting point: 214 – 216 °C; FT-IR: υ (cm^{-1}) = 3328, 3222, 2214, 1629, 768; ^{1}H NMR (300 MHz) δ 8.16 – 8.02 (m, 2H), 7.56 – 7.41 (m, 4H), 7.39 – 7.16 (m, 3H, 1H $CDCl_3$), 5.43 (br. s, 2H), 2.06 (s, 3H). ^{13}C NMR (101 MHz) δ 163.6 (d, *J* = 250.4 Hz), 158.3, 151.6, 150.9, 144.2, 138.7, 130.6 (d, *J* = 8.5 Hz), 129.9 (d, *J* = 3.3 Hz), 129.0, 126.3, 121.5, 116.7, 115.9 (d, *J* = 22.0 Hz), 109.5, 88.5, 14.8. ^{19}F NMR (282 MHz) δ -110.51; HRMS calcd. for $C_{20}H_{14}FN_5$ [M^+] 343.1233, found. 343.1244.

6-amino-3-methyl-4-(3-nitrophenyl)-1-phenyl-1H-pyrazolo[3,4-b]pyridine-5-carbonitrile (1j):

Isolated as white solid, (315 mg, 85%), R_f: 0.52, Melting point: 157 – 159 °C; FT-IR: υ (cm^{-1}) = 3357, 3224, 2216, 1617, 753; ^{1}H NMR (400 MHz) δ 8.46 (m, 1H), 8.38 (t, *J* = 1.8 Hz, 1H), 8.19 – 8.02 (m, 2H), 7.89 – 7.77 (m, 2H), 7.58 – 7.46 (m, 2H), 7.34 (m, 1H), 5.55 (br. s, 2H), 2.04 (s, 3H). ^{13}C NMR (75 MHz) δ 158.2, 149.4, 148.1, 143.6, 138.5, 138.1, 135.6, 134.5, 130.0, 129.0, 126.5, 124.8, 123.9, 122.8, 121.6, 116.2, 88.2, 14.8; HRMS calcd. for $C_{20}H_{14}N_6O_2$ [M^+] 370.1178, found. 393.1195.

6-amino-4-(4-methoxyphenyl)-3-methyl-1-phenyl-1H-pyrazolo[3,4-b]pyridine-5-carbonitrile (1k):

Isolated as white solid, (323 mg, 91%), R_f: 0.47, Melting point: 195 – 197 °C; FT-IR: υ (cm^{-1}) = 3353, 3224, 2216, 1629, 765 ; ^{1}H NMR (400 MHz) δ 8.17 – 8.04 (m, 2H), 7.52 – 7.46 (m, 2H), 7.44 – 7.39 (m, 2H), 7.33 – 7.27 (m, 1H), 7.09 – 7.05 (m, 2H), 5.40 (br. s, 2H), 3.90 (s, 3H), 2.10 (s, 3H). ^{13}C NMR (101 MHz) δ 160.9, 158.4, 152.8 , 151.0, 144.5, 138.8, 130.2, 129.0, 126.1 (2C), 121.5, 117.2, 114.0, 109.7, 88.5, 55.4, 15.0.

6-amino-4-(2,6-difluorophenyl)-3-methyl-1-phenyl-1H-pyrazolo[3,4-b]pyridine-5-carbonitrile (1l):

Isolated as white solid, (307 mg, 85%), R_f: 0.55, Melting point: 227 – 229 °C; FT-IR: υ (cm^{-1}) = 3318, 3202, 2213, 1630, 768; ^{1}H NMR (300 MHz) δ 8.17 – 8.04 (m, 2H), 7.62 – 7.45 (m, 3H), 7.36 – 7.27 (m, 1H), 7.19 – 7.10 (m, 2H), 5.43 (br. s, 2H), 2.11 (s, 3H). ^{13}C NMR (101 MHz) δ 159.54 (dd, *J* = 252.0, 6.0 Hz), 158.2, 150.9, 143.9, 139.7, 138.6, 132.4 (t, *J* = 10.0 Hz), 129.0, 126.3, 121.6, 116.0, 112.0 (dd, *J* = 19.5, 6.0 Hz), 111.3 (t, *J* = 20.0 Hz), 110.0, 89.9, 13.0. ^{19}F NMR (282 MHz) δ -111.00; HRMS calcd. for $C_{20}H_{13}F_2N_5$ [M^+] 361.1139, found. 361.1151.

6-amino-3-methyl-4-(naphthalen-1-yl)-1-phenyl-1H-pyrazolo[3,4-b]pyridine-5-carbonitrile (1m):

Isolated as white solid, (319 mg, 85%), R_f: 0.55, Melting point: 195 – 197 °C; FT-IR: υ (cm^{-1}) = 3385, 3319, 2210, 1621, 776; ^{1}H NMR (300 MHz) δ 8.19 – 8.11 (m, 2H), 8.07 – 7.95 (m, 2H), 7.64 (dd, *J* = 8.2, 7.1 Hz, 1H), 7.59 – 7.43 (m, 26H), 7.36 – 7.28 (m, 1H), 5.47 (br. s, 2H), 1.59 (s, 3H). ^{13}C NMR (101 MHz) δ 158.5, 151.5, 150.7, 144.7, 138.8, 133.4, 131.6, 131.0, 130.2, 129.0, 128.6, 127.3, 126.6 (2C), 126.2, 125.2, 124.8, 121.5, 116.5, 110.8, 89.7, 13.4; HRMS calcd. for $C_{24}H_{17}N_5$ [M^+] 375.1484, found. 375.1503.

6-amino-3-methyl-4-(naphthalen-2-yl)-1-phenyl-1H-pyrazolo[3,4-b]pyridine-5-carbonitrile (1n):

Isolated as white solid, (338 mg, 90%), R_f: 0.58, Melting point: 270 – 272 °C; FT-IR: υ (cm^{-1}) = 3356, 3219, 2217, 1623, 744; ^{1}H NMR (300 MHz) δ 8.19 – 8.06 (m, 12H), 8.03 (d, *J* = 8.5 Hz, 1H), 7.99 – 7.92 (m, 3H), 7.66 – 7.47 (m, 5H), 7.35 – 7.27 (m, 1H), 5.45 (br. s, 2H), 2.02 (s, 31H). ^{13}C NMR (101 MHz) δ 158.4, 152.7, 150.9, 144.5, 138.8, 133.7, 132.7, 131.4, 129.0, 128.5 (2C), 128.0, 127.4, 127.0, 126.2, 125.7, 121.6, 116.9, 109.7, 88.7, 14.8; HRMS calcd. for $C_{24}H_{17}N_5$ [M^+] 375.1484, found. 375.1501.

6-amino-4-(3,5-difluorophenyl)-3-methyl-1-phenyl-1H-pyrazolo[3,4-b]pyridine-5-carbonitrile (1o):

Isolated as white solid, (314 mg, 87%), R_f: 0.67, Melting point: 198 – 200 °C; FT-IR: υ (cm^{-1}) = 3348, 3227, 2219, 1632, 744; ^{1}H NMR (300 MHz) δ 8.17 – 8.06 (m, 2H), 7.57 – 7.48 (m, 2H), 7.37 – 7.30 (m, 1H), 7.12 – 6.97 (m, 3H), 5.47 (br. s, 2H), 2.10 (s, 3H). ^{13}C NMR (126 MHz) δ 162.89 (dd, *J* = 252.0, 13.0 Hz), 158.2, 150.8, 149.6, 143.8, 138.6, 136.9 (t, *J* = 10.0 Hz), 129.0, 126.4, 121.5, 116.1, 112.1 (dd, *J* = 20.0, 7.0 Hz), 109.1, 105.5 (t, *J* = 25.0 Hz), 88.1, 14.5; ^{19}F NMR (376 MHz) δ -107.5; HRMS calcd. for $C_{20}H_{13}F_2N_5$ [M^+] 361.1139, found. 361.1150.

6-amino-4-(3,4-difluorophenyl)-3-methyl-1-phenyl-1H-pyrazolo[3,4-b]pyridine-5-carbonitrile (1p):

Isolated as white solid, (322 mg, 89%), R_f: 0.57, Melting point: 203 – 205 °C; FT-IR: υ (cm^{-1}) = 3369, 3227, 2215, 1634, 764; ^{1}H NMR (300 MHz) δ 8.15 – 8.08 (m, 2H), 7.56 – 7.48 (m, 2H), 7.43 – 7.30 (m, 3H), 7.27 – 7.21 (m, 1H), 5.46 (br. s, 2H), 2.10 (s, 3H). ^{13}C NMR (126 MHz) δ 158.2, 151.4 (dd, *J* = 252.6, 12.2 Hz), 150. 9, 150.24 (dd, *J* = 251.6, 12.8 Hz), 150.0 (d, *J* = 0.9 Hz), 143.8, 138.6, 130.7 (dd, *J* = 6.0, 4.3 Hz), 129.0, 126.3, 125.2 (dd, *J* = 6.6, 4.0 Hz), 121.5, 118.1 (dd, *J* = 25.0, 18.0 Hz), 116.3, 109.3, 88.4, 14.7; ^{19}F NMR (376 MHz) δ -135.15 (dd, *J* = 311.5, 21.3 Hz); HRMS calcd. for $C_{20}H_{13}F_2N_5$ [M^+] 361.1139, found. 361.1152.

6-amino-4-(4-cyanophenyl)-3-methyl-1-phenyl-1H-pyrazolo[3,4-b]pyridine-5-carbonitrile (1q):

Isolated as white solid, (326 mg, 93%), R_f: 0.50, Melting point: 237 – 239 °C; FT-IR: υ (cm^{-1}) = 3338, 3216, 2228, 2211, 1619; ^{1}H NMR (300 MHz) δ 8.13 – 8.06 (m, 2), 7.93 – 7.85 (m, 2H), 7.65 – 7.58 (m, 2H), 7.55 – 7.47 (m, 2H), 7.36 – 7.29 (m, 1H), 5.47 (br. s, 2H), 2.02 (s, 3H). ^{13}C NMR (126 MHz) δ 158.2, 150.9, 150.0, 143.6, 138.6, 132.5, 129.5, 129.0, 126.4, 121.5, 117.9, 116.2, 114.1, 109.0, 88.0, 14.7; HRMS calcd. for $C_{21}H_{14}N_6$ [M^+] 350.1280, found. 350.1303.

Acknowledgment

We thank Bu-Ali Sina University, Iran National Science Foundation (INSF) (Grant Number: 95831207), National Elites Foundation, University of Alicante (VIGROB-173, UAUSTI16-03), and the Spanish Ministerio de Economía y Competitividad (CTQ2015-66624-P) for financial support to our research groups.

Keywords: Pyrazolo[3,4-*b*]-pyridine, nanomagnetic catalyst, Fe_2O_3@$SiO_2(CH_2)_3$-Cl[DABCO-NO_2]$C(NO_2)_3$, solvent free, anomeric based oxidation.

References:

[1] O. Deutschmann, H. Knözinger, K. Kochloefl, T. Turek, *Heterogeneous Catalysis and Solid Catalysts*, Wiley-VCH Verlag GmbH & Co. KGaA, Weinheim, **2009** doi:10.1002/14356007.a05_313.pub2.

[2] M. A. Zolfigol, T. Azadbakht, V. Khakyzadeh, R. Nejatyami, D.M. Perrin, *RSC Adv*. **2014**, *4*, 40036–40042.

[3] a) M. A. Zolfigol, V. Khakyzadeh, A. R. Moosavi-Zare, A. Rostami, A. Zare, N. Iranpoor, M. H. Beyzavi, R. Luque, *Green Chem.* **2013**, *15*, 2132–2140; b) H. Sharghi, A. Khoshnood, M. M. Doroodmand, R. Khalifeh, *J. Iran Chem. Soc.* 2012, 9, 231–250; c) H. Sharghi, A. Khoshnood, R. Khalifeh, M. M. Doroodmand, *Mol. Divers.* 2015, 19, 481–500.

[4] S. B. Sapkal, K.F. Shelke, B.B. Shingate, M.S. Shingare, *Tetrahedron Lett.* **2009**, *50*, 1754–1756.

[5] a) M. Fallah-Mehrjardi, Mini-Rev. *Org. Chem.* **2017**, *14*, 122–129; b) M. Mokhtary, *J. Iran. Chem. Soc.* **2016**, *13*, 1827–1845.

[6] a) V. Polshettiwar, R. Luque, A. Fihri, H. Zhu, M. Bouhrara, J. M. Basset, *Chem. Rev*. **2011**, *111*, 3036–3075; b) B. Karimi, F. Mansouri, H. M. Mirzaei, *ChemCatChem* **2015**, *7*, 1736–1789; c) D. Zhang, C. Zhou, Z. Sun, L. Z. Wu, C. H. Tung, T. Zhang, *Nanoscale* **2012**, *4*, 6244–6255; d) M. B. Gawande, P. S. Branco, R. S. Varma, *Chem. Soc. Rev.* **2013**, *42*, 3371–3393; e) S. Hu, Y. Guan, Y. Wang, H. Han. *Appl. Energ.* **2011**, *88*, 2685–2690.

[7] A. Khazaei, M. A. Zolfigol, A. R. Moosavi‐Zare, J. Afsar, A. Zare, V. Khakyzadeh, M. H. Beyzavi, *Chin. J. Catal*. **2013**, *34*, 1936–1944.

[8] a) M. A. Zolfigol, M. Yarie, *RSC Adv.* **2015**, *5*, 103617–103624; b) H. Sharghi, A. Khoshnood, M. M. Doroodmand, Reza Khalifeh, *J. Heterocyclic Chem.* 2016, 53, 164–174.

[9] E. Juaristi, G. Cuevas, *Tetrahedron* **1992**, *48*, 5019–5087.

[10] S. A. Glover, *Tetrahedron* **1998**, *54*, 7229–7271.

[11] E. Juaristi, Y. Bandala, *Adv. Heterocyclic Chem.* **2012**, *105*, 189–222.

[12] C. M. Filloux, *Angew. Chem. Int. Ed.* **2015**, *54*, 8880–8894.

[13] M. Yarie, *Iran. J. Catal.* **2017**, *7*, 85–88.

[14] G. Hamasaka, H. Tsuji, Y. Uozumi, *Synlett* **2015**, *26*, 2037–2041.

[15] T. He, R. Shi, Y. Gong, G. Jiang, M. Liu, S. Qian, Z. Wang, *Synlett* **2016**, *27*, 1864–1869.

[16] C.-B. Bai, N.-X. Wang, Y. Xing, X.-W. Lan, *Synlett* **2017**, *28*, 402–414.

[17] N-X. Wang, J. Zhao, *Synlett*, 2007, 2785–2791.

[18] L. F. Pedrosa, W. P. de Macedo, A. C. R. Furtado, G. P. Guedes, J. C. Borges, J. A. L. C. Resende, M. G. F. Vaz, A. M. R. Bernardino, M. C. de Souza, *ARKIVOC* **2014**, *iv*, 38–50.

[19] V. Kumar, K. Kaur, G. K. Gupta, A. K. Sharma, *Eur. J. Med. Chem.* **2013**, *69*,735–753.

[20] D.-Q. Shi, H. Yao, J.-W. Shi, *Synth. Commun.* **2008**, *38*, 1662–1669.

[21] I. H. Eissa, A. M. El-Naggar, M. A. El-Hashash, *Bioorg. Chem*. **2016**, *67*, 43–56.

[22] T. I. El-Emary, *J. Chin. Chem. Soc*. **2007**, *54*, 507–518.

[23] X. Zhang, X. Li, X. Fan, X. Wang, J. Wang, G. Qu. *Aust. J. Chem.* **2009**, *62*, 382–388.

[24] Y. L. Chen, International Patent WO 9534563 A1 (1995); Chem. Abstr., 124, 232447 (1995).

[25] J. Quiroga, S. Cruz, B. Insuasty, R. Abonia, *J. Heterocycl. Chem.* **2001**, *38*, 53–60.

[26] B. Zhao, Y. Li, P. Xu, Y. Dai, C. Luo, Y. Sun, J. Ai, M. Geng, W. Duan. *ACS Med. Chem. Lett.* **2016**, *7*, 629–634.

[27] M. D. Hill, H. Fang, J. M. Brown, T. Molski, A. Easton, X. Han, R. Miller, M. Hill-Drzewi, L. Gallagher, M. Matchett, M. Gulianello, A. Balakrishnan, R. L. Bertekap, K. S. Santone, V. J. Whiterock, X. Zhuo, J. J. Bronson, J. E. Macor, A. P. Degnan, *ACS Med. Chem. Lett.* **2016**, *7*, 1082–1086.

[28] M. A. Zolfigol, A. Khazaei, S.; Alaie, S. Baghery, F. Maleki, Y. Bayat, A. Asghari, *RSC Adv*. **2016**, *6*, 58667–58679.

[29] M.A. Zolfigol, H. Gholami, V. Khakyzadeh, *Principles of organic synthesis with a new approach*, Third Ed., Bu-Ali Sina University Publishers, Hamedan, Iran, **2014**, p. 26.

[30] S. J. Angyal, K. James, *Aust. J. Chem.* **1970**, *23*, 1209–1221.

[31] a) J. M. Erhardt, J. D. Wuest, *J. Am. Chem. Soc*. **1980**, *102*, 6363–6364; b) T. J. Atkins, *J. Am. Chem. Soc*., **1980**, *102*, 6364–6365; c) J. M. Erhardt, E. R. Grover, J. D. Wuest, *J. Am. Chem. Soc*., **1980**, *102*, 6365–6369.

[32] a) M. A. Zolfigol, F. Afsharnadery, S. Baghery, S. Salehzadeh, F. Maleki, *RSC Adv*. **2015**, *5*, 75555–75568; b) M. A. Zolfigol, M. Safaiee, F. Afsharnadery, N. Bahrami-Nejad, S. Baghery, S. Salehzadeh, F. Maleki, *RSC Adv*. **2015**, *5*, 100546–100559.

[33] A. R. Moosavi-Zare, M. A. Zolfigol, Z. Rezanejad *Can. J. Chem.* **2016**, *94*, 626–630; d) M.A. Zolfigol, M. Kiafar, M. Yarie, A. Taherpour, M. Saeidi-Rad, *RSC Adv*. **2016**, *6*, 50100–50111.

[34] a) M.A. Zolfigol, M. Yarie, *Appl. Organometal. Chem*. **2017**, *31*, e3598, DOI: 10.1002/aoc.3598; b) M. A. Zolfigol, M. Kiafar, M. Yarie, A. Taherpour, T. Fellowes, A.N. Hancok, A. Yari, *J. Mol. Struct.* **2017**, *1137*, 674-680.

[35] M. Kiafar, M. A. Zolfigol, M. Yarie, A. Taherpour, *RSC Adv*. **2016**, *6*, 102280–102291.

[36] M. A. Zolfigol, M. Safaiee, B. Ebrahimghasri, S. Baghery, S. Alaie, M. Kiafar, A. Taherpour, Y. Bayat, A. Asgari, *J. Iran. Chem. Soc*. **2017**, *14*, 1839–1852.

[37] S. Baghery, M. A. Zolfigol, F. Maleki, *New J. Chem*. **2017**, *41*, 9276–9290.

[38] a) N. Koukabi, E. Kolvari, A. Khazaei, M. A. Zolfigol, B. S. Shaghasemi, H. R. Khavasi, *Chem. Commun*. **2011**, *47*, 9230–9232; b) N. Koukabi, E. Kolvari, M. A. Zolfigol, A. Khazaei, B. S. Shaghasemi, B. Fasahati, *Adv. Synth. Catal.* **2012**, *354*, 2001–2008; c) T. Azadbakht, M. A. Zolfigol, R. Azadbakht, V. Khakizadeh, D. Perrin, *New J. Chem*. **2015**, *39*, 439–444; d) M. Safaiee, M. A. Zolfigol, F. Afsharnadery, S. Baghery, *RSC Adv*. **2015**, *5*, 102340–102349; e) M. A. Zolfigol, M. Kiafar, M. Yarie, A. A. Taherpour M. Saeidi-Rad, *RSC Adv*. **2016**, *6*, 50100–50111; f) M. Yarie, M. A. Zolfigol, Y. Bayat, A. Asgari, D. A. Alonso, A. Khoshnood, *RSC Adv*. **2016**, *6*, 82842–82853; g) L. Mohammadi, M. A. Zolfigol, M, Ebrahiminia, K. P. Roberts, S. Ansari, T. Azadbakht, S. R. Hussaini, *Catal. Commun.* **2017**, *102*, 44–47.

Comentario [U3]: دکتر خشنود عزیز علت هایلایت شدن این رفرنس را متوجه نشدم بخاطر چیست.